SPAWAR

Systems Center
San Diego

TECHNICAL DOCUMENT 2993
January 1998

Tomographic Image Reconstruction of MCM Targets Using Synthetic Dolphin Signals

R. A. Altes
Chirp Corporation

P. W. Moore
D. A. Helweg
SSC San Diego

TECHNICAL DOCUMENT 2993
January 1998

Tomographic Image Reconstruction of MCM Targets Using Synthetic Dolphin Signals

R. A. Altes
Chirp Corporation

P. W. Moore
D. A. Helweg
SSC San Diego

SPAWAR

Systems Center San Diego

Space and Naval Warfare Systems Center
San Diego, CA 92152–5001

SPACE AND NAVAL WARFARE SYSTEMS CENTER
San Diego, California 92152–5001

H. A. Williams, CAPT, USN
Commanding Officer

R. C. Kolb
Executive Director

ADMINISTRATIVE INFORMATION

The work detailed in this document was performed for the Office of Naval Research, Code 235, under program element 0602315N. Contract N66001–97–M–U033 was carried out by the Chirp Corporation, 8248 Sugarman Drive, La Jolla, CA 92037, under the technical coordination of P. W. Moore and D. A. Helweg of Space and Naval Warfare Systems Center, San Diego, Research and Animal Care Branch, Code D351.

Released by
P. W. Moore, Head
Research and Animal Care
Branch

Under authority of
J. E. Haun, Head
Biosciences Division

SB

CONTENTS

Figures

1. INTRODUCTION

Back projection (BP) tomography is a technique for reconstructing an image from its projections. For x-rays, each projection sample is formed by an integration line that passes through the object to be imaged. The value of the projection sample is the absorption of the x-ray along the integration line. A projection is formed by a set of parallel integration lines. The corresponding projection line is orthogonal to the integration lines. Different projections are obtained by rotating the integration and projection lines relative to the object. For x-rays, the reconstructed image is a two-dimensional (2-D) representation of absorption at each point in the plane of rotation. Displacement of the plane of rotation along a line orthogonal to the plane yields a set of 2-D reconstructions that can be combined to form a 3-D image (Macovski, 1983; Rosenfeld & Kak, 1982).

For wideband sonar, radar, and ultrasound with fine range resolution, the echo amplitude vs. delay (A-scan) is another form of projection. If the echo amplitude at a given delay consists of the sum of the reflectivity from all points with the same delay, then the echo amplitude is a projection sample formed by a constant-delay integration surface (e.g., a spherical shell) that passes through the object to be imaged. The sum of point reflectivities is weighted by the beam pattern. The corresponding projection line is the range axis or the direction along which the beam pattern is maximized. Different projections are obtained by changing aspect angle with respect to the target (e.g., by rotating the target or moving the transmitter/receiver along a path orthogonal to the propagation direction). Synthetic aperture (SA) processing is a technique for constructing an image of an object from A-scans that are obtained at different aspect angles, i.e., from a sequence of projections (Munson, Obrien, & Jenkins, 1983).

If the beam pattern was sufficiently narrow such that cross-range (azimuth or elevation) resolution was as fine as range resolution, then SA processing would be unnecessary. Many wideband sonar/radar/ultrasound systems, however, have much finer resolution in the range direction than in cross-range. SA processing is a technique to convert such fine range resolution into fine cross-range resolution.

Appendix A shows that SA imaging and BP tomography can be made identical by applying a gradual high-pass filtering function to A-scan radar/sonar data. This equivalence between SA and BP has considerable practical and theoretical consequences. These consequences and their applications are discussed in the following sections.

2. THE POINT SPREAD FUNCTION AND THE RANGE, CROSS-RANGE AMBIGUITY FUNCTION (RCAF)

The point spread function of an imaging system is the representation of a single point (a 2-D impulse) by the system. For a finite aperture system, this representation is a smeared version of the point. This smeared version is obtained by 2-D convolution of the input point with the system point spread function.

For a finite aperture (spatially band-limited) system, image input data can be represented as a set of sample points with different amplitudes at a sequence of 2-D locations. For a linear system, the image of this input is obtained by 2-D convolution of the input with the system point spread function. The image is, thus, smeared or defocused by the point spread

function. A more accurate representation of the input data is obtained by using an imaging system with a point spread function that more closely resembles an impulse.

The point spread function of a BP image reconstruction system can be predicted by using the equivalence of BP and SAS. For a real or synthetic array, the imaging capability of a radar/sonar system is described by the range, cross-range ambiguity function (RCAF) of the system (Altes, 1979). An ambiguity function is the response of a receiver (e.g., a correlator or likelihood function generator) to a set of parameter hypotheses when the largest response is obtained for the correct parameter hypotheses. An accurate parameter estimator will have a large response for the correctly hypothesized parameter values and a small response for incorrect hypotheses. The ambiguity function of an accurate estimator will be an impulse-like function of the hypothesized parameter values. If the parameters are range and cross-range (azimuth or elevation), then a point target that is concentrated at a single range, cross-range position will be represented by a RCAF that is maximized at the position of the point target when this position is correctly hypothesized. A complete image is obtained by moving the hypothesized range-azimuth locations over the image plane. This movement of hypothesized parameters results in a convolution of the RCAF with a 2-D reflectivity function. The image of a scatterer that is composed of many point targets is a 2-D convolution of the reflector distribution with the RCAF.

The RCAF of a radar/sonar system operates in the same way as the point spread function of an optical system; 2-D convolution of the input distribution with the RCAF or point spread function determines the system's representation of an image. The RCAF is, thus, the point spread function of a radar/sonar imaging system. For a single transducer, the RCAF is determined by the autocorrelation function of the transmitted signal in the range direction and by the transducer beam pattern in the cross-range direction. The RCAF can be measured by moving a point target away from a hypothesized target location at the center of the transducer beam pattern and noting the receiver response to the target at different range and cross-range locations when the hypothesized location is unchanged . This measurement assumes that the receiver uses correlation (or likelihood function synthesis) in both range and cross-range. Correlation in the range direction is accomplished with temporal matched filtering, and correlation in the cross-range direction is accomplished with delay-and-sum beam forming for multi-element arrays. The RCAF of a single transducer will be called the "range-azimuth beam pattern" of the transducer/waveform combination.

For delay-and-sum beam forming, the RCAF for a real or synthetic array of transducers is the sum of the individual transducer range-azimuth beam patterns at the location of an imaged point. For a wideband, high-resolution sonar, any one beam pattern can be approximated by a line segment that is orthogonal to the propagation direction. The width (range extent) of the line segment is the range resolution cell of the sonar, and the line segment length (azimuth extent) is the transducer beam width. The beam width is typically much wider than the range resolution cell, yielding a line-like range-azimuth beam pattern. (If azimuth or cross-range resolution were as good as range resolution, there would be no need for back projection or synthetic aperture processing; the environment could be imaged from a single aspect angle.) The line segments corresponding to all the real or synthetic transducer locations intersect at a point being imaged (the hypothesized point target position), creating an asterisk-like pattern. This asterisk-like pattern is the sum of rotated range-azimuth beam patterns and is the point spread function or RCAF of a synthetic multistatic system composed of multiple transducers at different locations.

The SAS or BP image is the actual reflectivity distribution convolved or smeared by the asterisk-like point spread function (the RCAF). The peak-to-sidelobe ratio of the point spread function is a measure of how well the point spread function resembles an impulse, and is, thus, associated with image quality. For a synthetic aperture sonar or radar, the peak-to-sidelobe ratio is the number of different transducers or aspect angles (i.e., the sum of all the rotated line segments at their intersection divided by the height of one of the line segments).

3. SYSTEM TRADEOFFS

The effect of restricting the observation interval to, for example, 90 degrees rather than 360 degrees, can be assessed by analyzing the effect of such a restriction on the RCAF. If the bandwidth and angular sampling interval remain unchanged, then reducing the observation interval by a factor of four should reduce the peak-to-sidelobe ratio by a factor of four. The asterisk pattern is also affected; the sidelobes are restricted to a "bow tie" pattern that is 90 degrees wide on each side. The reduction in peak-to-sidelobe level results in smearing or defocusing of the image. To counteract this effect, more line segments within the bow tie can be added by sampling more often in angle, viz., four times as often. The peak-to-sidelobe ratio will then be the same as before, provided that the line segments are sufficiently narrow in width (range extent) so as not to overlap significantly (except at the center of the asterisk or bow tie) when they are rotated by only one-quarter of the initial angular sampling interval. To assure that additional overlap does not occur, the line-segment widths should be narrowed by increasing the bandwidth by a factor of four.

Given an image of independent point scatterers that is obtained over a 360-degree interval, an equivalent image can theoretically be obtained over an observation interval of 360/N degrees, provided that the angular sampling rate and the signal bandwidth are both multiplied by N. This result is consistent with an animal sonar system that attempts to obtain a high-quality acoustic image from echo data that are observed over a limited observation angle. The predicted behavior is to make the bandwidth as wide as possible and to increase the angular sampling rate. Echolocating dolphins move back and forth near an object that they are trying to identify (Gisiner, 1994), while emitting echolocation clicks at an extremely high repetition rate (Moore et al., 1990; Roitblat et al., 1991). This behavior increases the angular sampling frequency for a restricted observation interval. The dolphin's echolocation bandwidth is also effectively increased via higher SNR and lower high-frequency attenuation associated with proximity to a target.

Ambiguity function analysis thus indicates a tradeoff between angular observation interval and bandwidth for target imaging. A smaller aspect interval can be compensated by increased bandwidth, along with increased angular sampling rate. At long range, increased angular sampling rate can be obtained by transmitting a sequence of decorrelated signals (e.g., linear-frequency-modulated signals with different chirp rates).

4. ROTATED WAVELET ANALYSIS

Another practical problem is obtaining a high-quality image with sparse angular sampling from a relatively small number of aspect angles. In terms of the point spread function or RCAF, the problem is to design an imaging system with an impulse-like point spread function, even though aspect angles may be separated by, for example, 30 degrees. This goal can be accomplished by using range-azimuth beam patterns with a particular sidelobe

structure. Negative sidelobes occur naturally with finite-length transducers and with signals that have no power at zero frequency. The object is to design these sidelobes so that a sum of rotated range-azimuth beam patterns is impulse-like. Each beam pattern should be cancelled by the negative sidelobes of its rotated neighbors except at the point of rotation, which corresponds to the center of each beam pattern. The 2-D Fourier transform of an impulse is a constant over the system bandwidth. The Fourier sum transforms of the rotated range-azimuth beam patterns (after space-time matched filtering) should, thus, be constant over the system bandwidth. This design criterion is similar to wavelet analysis, except that the basis functions are 2-D range-azimuth beam patterns that are rotated rather than scaled. The required range-azimuth beam patterns are easily obtained via 2-D Fourier transform analysis, and they resemble the measured versions of such patterns that are observed around an echolocating dolphin (Altes, 1995).

5. PARTIAL IMAGE RECONSTRUCTION FROM PROJECTIONS

It is not clear how to construct only part of an image with conventional back projection, but the equivalence to SAS makes such construction straightforward. To investigate part of a scene, the synthetic array focuses on each point contained in the area of interest and disregards all other areas. Focusing is accomplished by delay-and-sum beamforming.

6. FEATURE IMAGES

The usual SAR/SAS/BP radar/sonar image is a representation of target reflectivity as a function of position (pixel location). Other features, however, are important for target identification and target/clutter discrimination. Such features include the echo bandwidth, echo center frequency, and texture (e.g., the relative number of large and small maxima in a small interval surrounding a given location, etc). These features can be extracted from each echo and represented as a function of delay, yielding a generalized A-scan display of feature value vs. range. These generalized projections can be combined to form a high-resolution SAS/BP image of the feature value as a function of pixel location. Feature images can accentuate or deaccentuate clutter relative to a standard reflectivity image, and difference images that greatly enhance signal-to-clutter ratio (SCR) can be constructed. Some examples are presented in section 8.

Different feature images comprise spatially registered maps of the acoustic environment. Combining these images (e.g., by forming weighted differences between them) is equivalent to forming a composite image from different features at the same location. This type of representation and combination is found in the superior colliculus of mammals (Drager & Hubel, 1975) and the optic tectum of reptiles (Hartline, Kass, & Loop, 1978) and fish (Bastian, 1986). Overlaid neuronal feature maps are derived from different sensors (e.g., vision and infrared in the rattlesnake). Large neurons penetrate the spatially registered maps to combine features at a given environmental location. These neurons implement a biological version of sensor fusion.

7. THREE-DIMENSIONAL REPRESENTATIONS

Different projections are obtained when an object is rotated relative to a transmiter/receiver (e.g., when the object or the radar/sonar platform moves in a direction that is orthogonal to the propagation direction). In many practical situations, the platform is above the plane of rotation. This displacement in elevation allows for a 3-D representation of target

reflectivity. To construct a 2-D image, the elevation of the corresponding image plane must be specified. A sequence of spatially registered 2-D images is obtained for different specified elevations. These images can be included in the set of spatially registered feature maps that are combined to form a composite image with increased SCR. Elevation can, thus, be treated as another feature in a set of feature maps.

Extra information from elevation can be used to adaptively improve focusing and to construct a 3-D surface that represents the physical shape of an object as it would be perceived with vision. Such a surface is different from a representation of reflectivity as a function of position, and it allows direct comparison with visual representations (e.g., photographs) of objects. A visual analogue would be very useful to an animal that tries to perform sensor fusion by combining spatially registered feature maps from vision and echolocation. There is some speculation that dolphins may be capable of such a vision-like target representation (Pack & Herman, 1995), although the issue of the cognitive representation of targets formed by echolocating dolphins remains open to debate (Helweg et al., 1996; Harley et al., 1995; Roitblat et al., 1995), and the lay concept of "seeing with echolocation" remains unsubstantiated. However, a vision-like target representation is well-suited to human observers and could have application to improvement of MCM performance.

8. EXAMPLES AND APPLICATIONS

Sonar echoes from a rotating ONI-certified ROCKAN mine simulator were collected in Lake Travis by the Applied Research Laboratory at the University of Texas in Austin, Texas. When seen from above, the target resembles a trapezoid with small fins or tabs at the corners of the base (figure 1). The target was suspended at a 45° angle so that it was not totally contained within the plane of rotation. The sonar receiver was 7 m above the plane of rotation and was at a depth of 3 m. The center of rotation was 31 m from the sonar transducer. The signal was a broadband bottlenose dolphin echolocation click typical of echolocation signals used by U.S. Navy dolphins (Moore, 1997). The digitized click and its spectrum is presented in figure 1a. Echoes were digitized at a sampling frequency of 500 kHz, and observation angles were separated by approximately 0.36 degrees.

The echo from each aspect angle was processed with a filter that yielded a minimum mean-square error estimate of the target impulse response. This filter was a cascade of an inverse filter and a Wiener filter (Turin, 1957; Altes, 1977). For frequency domain components with high signal-to-noise (SNR), the filter transfer function approximates the inverse of the signal spectrum. At low SNR, the filter transfer function approximates a matched filter. The filtered echoes from different aspects are A-scans or projections that are combined to form a SAS/BP image.

Figure 2 shows the resulting SAS/BP images before image-processing techniques (such as adaptive thresholding and contrast enhancement) were applied. These images are sufficient for demonstration purposes, but they do not exploit the full resolution capability of the system. Each image pixel incorporates 20 echo samples and, thus, represents a volume element that is 3 cm on a side. Every tenth echo was used, so the observation angles were separated by approximately 3.6 degrees. The elevation of the image plane in figure 2 was chosen to maximize the variance of the pixel levels in the 2-D image and, thus, maximize a measure of overall sharpness or focus. The cloudiness of the image is associated with volume clutter (reverberation) that usually is caused by small air bubbles. In medical ultrasound,

such clutter is much more pronounced, and is called "speckle." Volume reverberation in sonar should become much stronger for buried objects and for turbulent water that contains more air bubbles and other particles.

The two images in figure 2 appear to be identical, but actually are slightly different. The left-hand image was derived from the absolute values of the echo samples. Each echo has a complex representation with the real part corresponding to the echo itself and the imaginary part corresponding to the Hilbert transform of the echo. The envelope of the echo is the magnitude of the complex representation (i.e., the square root of the sum of the squares of the real and imaginary parts). For a point target, the echo envelope is broader than the absolute value of the real part of the echo. For uniformly distributed clutter, this broadening should result in a slight decrease in SCR. Such a difference can be exploited by subtracting a weighted version of one image from the other and setting negative pixel values to zero. The resulting difference image can enhance the target SCR, as on the left-side of figure 3, or suppress it as on the right-side of figure 3. The negative contrast image on the right-side of figure 3 is often used in medical ultrasound and may prove to be important for finding buried sonar targets.

SCR also can be enhanced or suppressed by using feature images. Rough surfaces and volume reverberation can be discriminated from smooth surfaces by counting the number of relatively small echo maxima in a short delay interval. This number tends to be larger for rough surfaces and for volume reverberation. Figure 4 shows difference images that were constructed from a roughness feature image and a conventional reflectivity image. Volume clutter was deaccentuated and SCR was increased by subtracting a weighted roughness image from the conventional image and setting all negative pixels to zero. A negative contrast image that accentuates clutter and makes the target disappear was obtained by subtracting a weighted conventional image from the roughness image and setting all negative pixels to zero. The roughness feature was calculated by defining a "small" echo maximum to have an amplitude that is less than one-tenth the amplitude of the largest echo maximum in a short delay interval. The delay interval consisted of 10 echo samples on either side of each imaged point. Because each image pixel incorporated 20 of the original echo samples, the interval for feature measurement is uniquely associated with each image pixel.

The target did not lie within a single constant-elevation plane, and many parts of the target were not well focused when an elevation with best overall focus was selected for the imaging system. The focus at each point was optimized by constructing a composite image consisting of pixels from many image planes at different elevations. At each location in the image, the pixel with the best individual focus was selected from the different representations of the same pixel in image planes at various elevations. For an image plane at a specified elevation, a measure of individual pixel focus was the sum of the magnitudes of the differences between the pixel value and the values of surrounding pixels. This measure was used to construct the composite image on the right-hand side of figure 5. The image on the left-hand side of figure 5 is a conventional single-elevation image (chosen from the elevation that maximizes an overall focus measure) that was passed through an adaptive threshold. Pixels with values that were less than the threshold value were set to zero. The right-hand image is constructed by selecting pixels with best individual focus from the left-hand image and from other images constructed with different elevation hypotheses. The resulting image appears to be better focused than the conventional image.

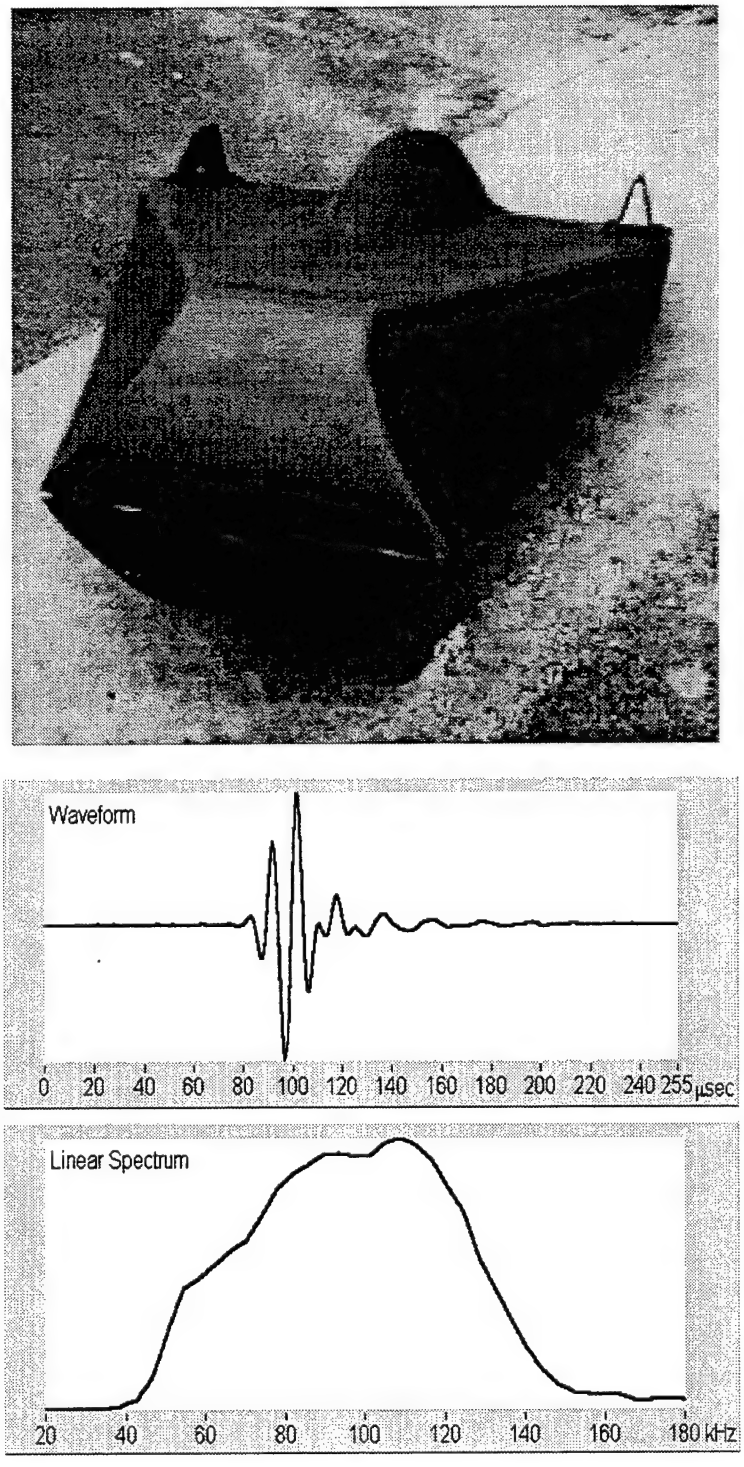

Figure 1. The target, an ONI-certified ROCKAN very shallow water (VSW) mine simulator, is presented in the top panel. The outer shell is fiberglass. The bottom panels depict the dolphin biosonar click used to ensonify the ROCKAN and its associated linear spectrum. Click duration was approximately 70 msec, with a peak frequency of approximately 110 kHz.

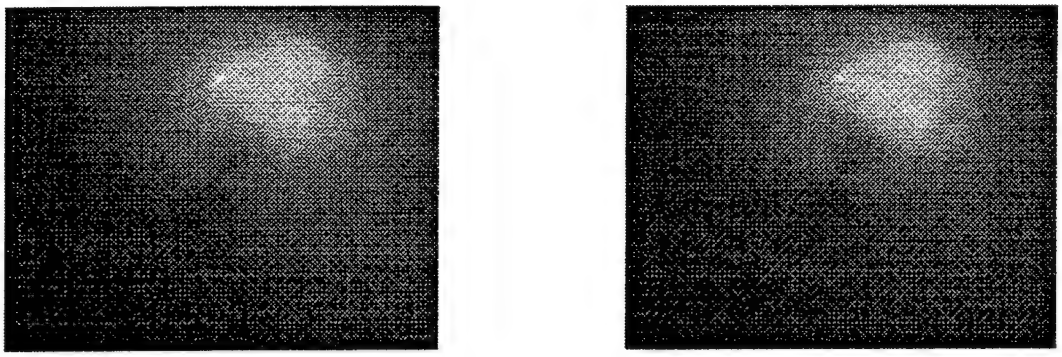

Figure 2. Two SA or BP representations of the target before adaptive thresholding and contrast enhancement.

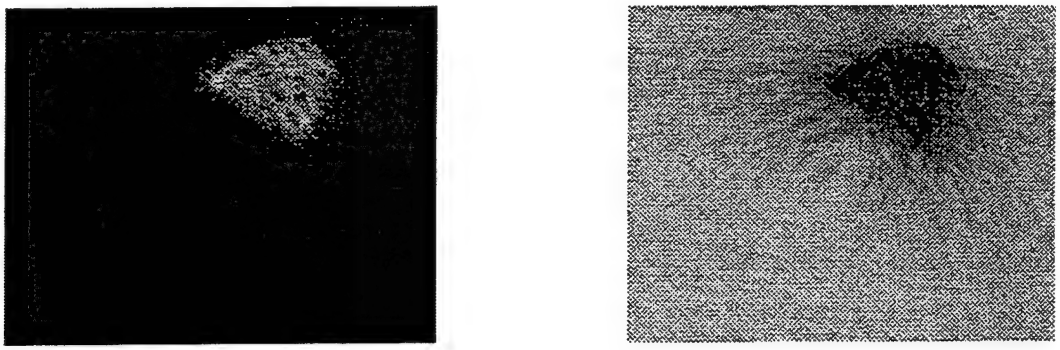

Figure 3. Target and clutter enhancement based on differences between the representations in figure 2.

Adaptive focusing as in figure 5 can be used to partially compensate for nonhomogeneous propagation media and other adverse effects. Image planes at multiple elevations provide redundancy that can be exploited with various image fusion or filtering criteria. For a buried target, adaptive combining of pixels from image planes at different elevations can be used to eliminate those elevations where SCR is comparatively low. A weighted sum of pixels from different closely spaced elevations may be preferable to selecting a pixel from one specific elevation.

Image planes at multiple specified elevations can also be used to estimate the physical shape of the target surface and, thus, to construct a vision-like target representation. This application depends on a criterion for recognizing a surface pixel. At present, the best surface recognition criterion maximizes reflectivity while constraining the gradient of reflectivity to be small in three dimensions. This criterion jointly maximizes reflectivity and a smoothness measure. Figure 6a shows a composite image that is constructed by selecting pixels with maximum surface recognition criterion from 40 different elevations. The corresponding

elevations are saved and used to construct a 3-D surface that represents the physical surface of the target. Figures 6b-6d show the resulting surface estimate from slightly different aspect angles. The whiteness of the surface is the reflectivity shown in figure 6a; the height of the surface is determined by the elevations of pixels that maximize the surface recognition criterion.

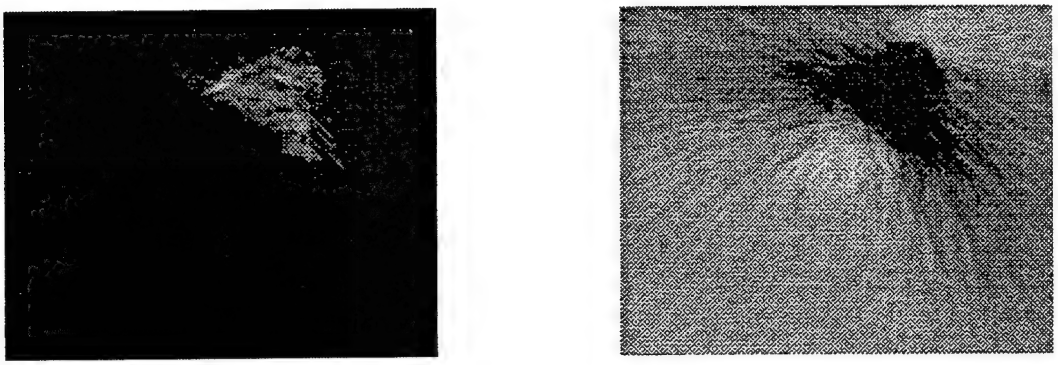

Figure 4. Difference images constructed from a conventional image of target reflectivity and a feature image of target roughness. A "smoothness" feature image is constructed by subtracting a weighted roughness feature image from a conventional image and setting negative pixel values to zero.

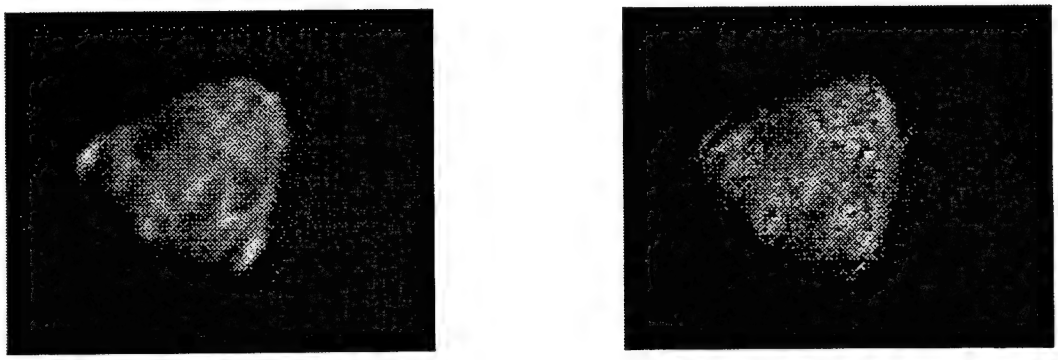

Figure 5. A conventional image from the elevation that maximizes an overall focus measure (left) and a composite image composed of pixels from multiple elevations, where a focus measure for each individual pixel is maximized (right).

Figure 6 illustrates the possibility of using 3-D acoustic imaging data to construct a physical replica of the target surface as it would be perceived visually. Such a representation should be extremely useful for human sonar operators. If echolocating animals were able to construct such a model, then acoustic data could be used to directly infer the visual shape of an object as suggested in Bastian (1986); c.f. Helweg et al. (1996); Harley et al. (1996); and Roitblat et al. (1995).

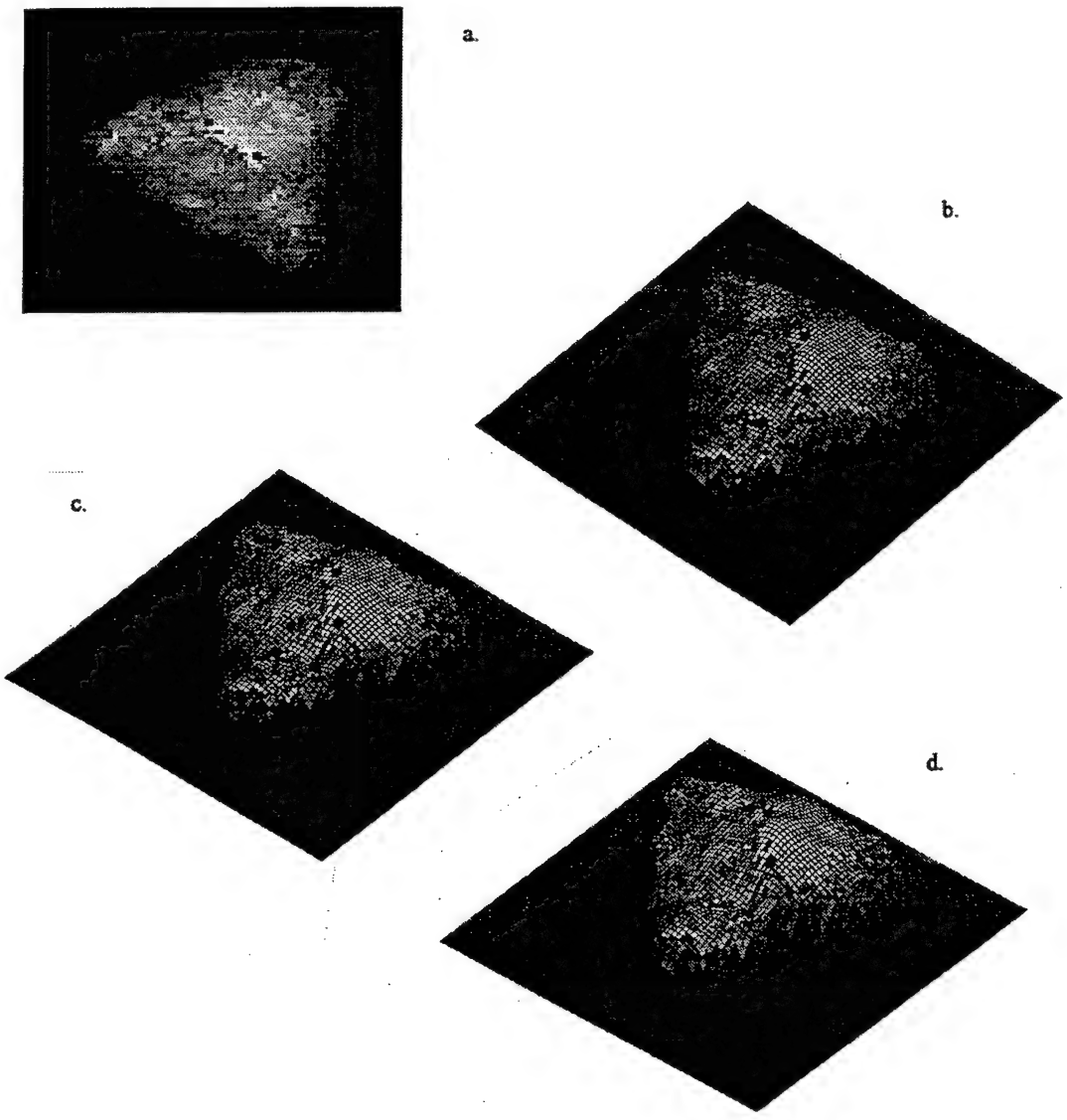

Figure 6. Figure 6a is a composite of pixels chosen from images at different elevations (z). Each pixel value in this image is the maximum value of a surface recognition criterion (maximized over z). Figures 6b through 6d are composite 3-D surface images seen from slightly different aspects. Surface height (z) is chosen from multiple images at different elevations; z is the elevation that maximizes the surface recognition criterion at a given location (x,y) in the image plane. The whiteness of the surface equals the corresponding value of the surface recognition criterion and is the same as in 6a. The goal is to use 3-D acoustic imaging information to construct a version of the target that resembles a visual representation of the target's surface.

9. ALGORITHM EFFICIENCY

Synthetic aperture and back propagation yield identical images, but typically use different processing algorithms. There appears to be no advantage to using BP algorithms for SA imaging if appropriate quantities are pre-computed for synthetic aperture so as to avoid needless, iterative computation of the same quantity. When such preprocessing is used, a PC with a 166 MHz clock rate can process a new echo every 3 sec. This rate approaches real-time computation, especially if faster, dedicated processors are used. The image is sequentially synthesized by this process, and it can be evaluated before the process is completed. Such evaluation, along with the capability to estimate part of an image, should also save time and increase area coverage rate.

10. CONCLUSIONS

The equivalence of back projection and synthetic aperture imaging can be exploited to obtain the following advantages:

1. Theoretical tradeoff predictions can be made by considering the effect of decreased angular observation interval or angular sampling rate on the peak-to-sidelobe ratio of the point spread function. These predictions also indicate the payoff associated with large signal bandwidth.
2. If transducers and transmitted waveforms are designed to make the range-azimuth beam pattern the same as a rotated wavelet basis function, then high-quality images can be obtained with a substantial reduction in angular sampling rate (e.g., with observations separated by 30 degrees).
3. Images can be constructed sequentially, and there is no need to synthesize a complete image when only part of the image is of interest.
4. "Feature images" can be constructed by replacing the usual reflectivity feature by other localized features such as roughness measures and spectral descriptors.
5. Feature images can be combined with conventional reflectivity images to suppress or enhance clutter or targets with different properties (e.g., rough vs. smooth).
6. When the sonar transducer is located outside the plane of target rotation, elevation information is added to sonar images, allowing for 3-D imaging.
7. Elevation information can improve an image by selecting the best-focused version of the same pixel from image planes at different elevations.
8. Elevation information can be used to create a vision-like image of an object's surface by searching in elevation to find the pixel that maximizes a surface selection criterion and by storing the elevation at which the pixel was found. These elevation points define a surface that can be displayed to a human observer or used in an automatic pattern recognition system. A composite representation can be used to illuminate the surface with the corresponding reflectivity, thus identifying the parts of the surface that are most reflective. Such information can be used to design "stealthy" targets by identifying strongly reflective surface components.

9. Target images that are constructed with closely spaced hypothesized elevations can be combined via linear and nonlinear filters so as to maximize SNR and SCR for buried objects and turbulent propagation media.

11. REFERENCES

Altes, R. A. 1977. "Estimation of Sonar Target Transfer Functions in the Presence of Clutter and Noise," *Journal of the Acoustical Society of America* 61: 1371-1374.

Altes, R.A. 1979. "Target Position Estimation in Radar and Sonar, and Generalized Ambiguity Analysis for Maximum Likelihood Parameter Estimation," *Proceedings of IEEE* 67: 920-930, date, city, state where conference was held, publisher of proceedings.

Altes, R.A. 1992. "The Line Segment Transform and Sequential Hypothesis Testing in Dolphin Echolocation." In *Sensory Abilities of Aquatic Mammals,* pp. 317-355, J. Thomas, R. Kastelein, and A. Supin, Eds. Plenum, New York, NY.

Altes, R.A. 1995. "Signal Processing for Target Recognition in Biosonar," *Neural Networks* 8: 1275-1295.

Bastian, J. 1986."Electrolocation: Behavior, Anatomy, and Physiology." In *Electroreception,* pp. 577-612, T. H.. Bullock and W. Heilgenberg, Eds. Wiley, New York, NY.

Drager, U. C. and D. H. Hubel. 1975. "Responses to Visual Stimulation and relationship Between Visual, Auditory, and Somatosensory Inputs in Mouse Superior Colliculus," *Journal of Neurophysics* 38: 690-713.

Gisiner, R. 1994. "Videotape of Dolphin Behavior During Performance of a Target Discrimination Task." NRaD Bioacoustics Meeting. December 1994, San Diego, CA.

Harley, H. E., M. J. Xitco, and H. L. Roitblat. 1995. "Echolocation, Cognition, and the Dolphin's World." In *Sensory Systems of Aquatic Mammals,* pp. 529-542, R. A. Kastelein, J. A. Thomas, and P. E. Nachtigall, Eds. De Spil, Woerden, Netherlands.

Hartline, P. H., L. Kass, and M. S. Loop. 1978. "Merging of Modalities in the Optic Tectum: Infrared and Visual Integration in the Rattlesnake," *Science* 199: 1225-1229.

Helweg, D. A., W. W. L. Au, H. L. Roitblat, and P. E. Nachtigall. 1996. "Acoustic Basis for Recognition of Aspect-dependent Three-dimensional Targets by an Echolocating Bottlenose Dolphin," *Journal of the Acoustical Society of America* 99: 2409-2420.

Macovski, A. 1983. *Medical Imaging Systems*. Prentice-Hall, Englewood Cliffs, NJ.

Moore, P. W. B. 1997. "Mine Hunting Dolphins of the Navy." In *Detection and Remediation Technologies for Mines and Minelike Targets II. SPIE Proceedings Series*, 3079, date, location of conference.

Moore, P. W. B., H. L. Roitblat, R. H. Penner, and P. E. Nachtigall. 1990. "Recognizing Successive Dolphin Echoes with an Integrator Gateway Network," *Neural Networks* 4: 701-709.

Munson, D.C. Jr., J. D. O'Brien, and W. K. Jenkins. 1983. "A tomographic Formulation of Spotlight-mode Synthetic Aperture Radar," *Proceddings of IEEE,* **71:** 917-925.

Pack, A. A. and L. M. Herman. 1995. "Sensory Integration in the Bottlenosed Dolphin: Immediate Recognition of Complex Shapes Across the Senses of Echolocation and Vision," *Journal of the Acoustical Society of America.* 98: 722-733.

Roitblat, H. L., D. A. Helweg, and H. E. Harley. 1995. "Echolocation and Imagery." In *Sensory Systems of Aquatic Mammals,* pp. 171-182, R. A. Kastelein, J. A. Thomas, and P. E. Nachtigall, Eds. De Spil, Woerden, Netherlands.

Roitblat, H.L., P. W. B. Moore, P. E. Nachtigall, and R. H. Penner. 1991. "Natural Dolphin Echo Recognition Using an Integrator Gateway Network." In *Advances in Neural Information Processing Systems 3,* pp. 273-281, D. S. Touretsky and R. Lippman, Eds. Morgan Kaufmann, San Mateo, CA.

Rosenfeld, A. and A. C. Kak. 1982. *Digital Picture Processing*, 2nd Ed., vol. 1. Academic Press, Orlando, FL.

Turin, G. L. 1957. "On the Estimation in the Presence of Noise of the Impulse Response of a Random, Linear Filter," *IRE Trans. Inform. Theory* IT-3: 5-10.

APPENDIX A

Back Projection and Synthetic Aperture Processing

In order to compare back projection with synthetic aperture imaging, it is helpful to review some properties of two-dimensional Fourier transforms. The first property is the expression for the 2-D Fourier transform in cylindrical coordinates. In Cartesian coordinates, the 2-D Fourier transform is

$$f(x,y) = (2\pi)^{-2} \int_{-\infty}^{\infty} \int_{-\infty}^{\infty} F(\omega_x,\omega_y) \exp[j(\omega_x x + \omega_y y)] d\omega_x d\omega_y. \tag{A1}$$

In cylindrical (r,θ) frequency domain coordinates, $\omega_x = r\cos\theta$, $\omega_y = r\sin\theta$, and

$$F(\omega_x,\omega_y) = F(r\cos\theta, r\sin\theta) \equiv F_{cyl}(r,\theta). \tag{A2}$$

Cylindrical (ρ,ϕ) coordinates in the spatial domain are such that $x = \rho\cos\phi$, $y = \rho\sin\phi$, and

$$f(x,y) = f(\rho\cos\phi, \rho\sin\phi) \equiv f_{cyl}(\rho,\phi). \tag{A3}$$

Substituting equations (A2) and (A3) into equation (A1), changing variables , and noting that the Jacobian of the joint change of variables $\omega_x = r\cos\theta$, $\omega_y = r\sin\theta$ is

$$\begin{vmatrix} \partial\omega_x/\partial r & \partial\omega_y/\partial r \\ \partial\omega_x/\partial\theta & \partial\omega_y/\partial\theta \end{vmatrix} = \begin{vmatrix} \cos\theta & \sin\theta \\ -r\sin\theta & r\cos\theta \end{vmatrix} = |r|, \tag{A4}$$

yields

$$f_{cyl}(\rho,\phi) = (2\pi)^{-2} \int_{-\pi/2}^{\pi/2} \int_{-\infty}^{\infty} F_{cyl}(r,\theta) \exp[jr\rho(\cos\theta\cos\varphi + \sin\theta\sin\phi)] |r| dr d\theta. \tag{A5}$$

The desired expression for the 2-D Fourier transform in cylindrical coordinates is obtained by using the identity

$$\cos\theta\cos\phi + \sin\theta\sin\phi = \cos(\theta - \phi) \tag{A6}$$

in equation (A5), which results in

$$f_{cyl}(\rho,\phi) = (2\pi)^{-2} \int_{-\pi/2}^{\pi/2} \int_{-\infty}^{\infty} F_{cyl}(r,\theta) \exp[jr\rho\cos(\theta - \phi)] |r| dr d\theta. \tag{A7}$$

Rotation of an image in the x,y plane corresponds to a similar rotation of the 2-D Fourier transform of the image in the ω_x,ω_y plane. This property follows easily from equation (A7). Rotation in the x,y plane by γ radians transforms $f_{cyl}(\rho,\phi)$ to $f_{cyl}(\rho,\phi+\gamma)$. Replacing ϕ by ϕ+γ on the right-hand side of equation (A7) and changing variables by letting θ'=θ-γ, the right side becomes the 2-D Fourier transform of $F_{cyl}(r,\theta+\gamma)$. It follows that

$$f_{cyl}(\rho,\phi+\gamma) \leftrightarrow F_{cyl}(r,\theta+\gamma) \tag{A8}$$

or

$$f(x\cos\gamma - y\sin\gamma, y\cos\gamma + x\sin\gamma) \leftrightarrow F(\omega_x\cos\gamma - \omega_y\sin\gamma, \omega_y\cos\gamma + \omega_x\sin\gamma), \tag{A9}$$

where the double arrow indicates a 2-D Fourier transform pair.

Another property of 2-D Fourier transforms is that the projection of f(x,y) onto the x-axis is the 1-D inverse Fourier transform of $F(\omega_x,0)$. The projection of f(x,y) onto the x-axis is

$$P_0(x) \equiv \int_{-\infty}^{\infty} f(x,y)dy. \tag{A10}$$

Integrating

$$f(x,y) = (2\pi)^{-2}\int_{-\infty}^{\infty}\int_{-\infty}^{\infty} F(\omega_x,\omega_y)\exp[j(\omega_x x + \omega_y y)]d\omega_x d\omega_y$$

with respect to y yields

$$P_0(x) \equiv \int_{-\infty}^{\infty} f(x,y)dy = (2\pi)^{-1}\int_{-\infty}^{\infty} F(\omega_x,\omega_y)\exp(j\omega_x x)\delta(\omega_y)d\omega_x d\omega_y$$

$$= (2\pi)^{-1}\int_{-\infty}^{\infty} F(\omega_x,0)\exp(j\omega_x x)d\omega_x\,, \tag{A11}$$

which is the 1-D inverse Fourier transform of $F(\omega_x,0)$. It follows that

$$\int_{-\infty}^{\infty} P_0(x)\exp(-j\omega_x x)dx = F(\omega_x,0). \tag{A12}$$

The above projection property can be generalized to rotated versions of f(x,y). Rotating f(x,y) by θ radians yields

$$f_\theta(x,y) \equiv f(x\cos\theta - y\sin\theta, y\cos\theta + x\sin\theta). \tag{A13}$$

It follows from equation (A9) that the 2-D Fourier transform of $f_\theta(x,y)$ is a similarly rotated version of $F(\omega_x,\omega_y)$:

$$f_\theta(x,y) \leftrightarrow F_\theta(\omega_x,\omega_y) \equiv F(\omega_x\cos\theta - \omega_y\sin\theta, \omega_y\cos\theta + \omega_x\sin\theta). \tag{A14}$$

Letting $P_\theta(x)$ denote the projection of $f_\theta(x,y)$ onto the x-axis, i.e.,

$$P_\theta(x) \equiv \int_{-\infty}^{\infty} f_\theta(x,y)dy\,, \tag{A15}$$

equations (A10) through (A12) imply that the 1-D Fourier transform of $P_\theta(x)$ is $F_\theta(\omega_x,0)$. Using r instead of ω_x,

$$\int_{-\infty}^{\infty} P_\theta(x)\exp(-jrx)dx = F_\theta(r,0) = F(r\cos\theta, r\sin\theta) \equiv F_{cyl}(r,\theta). \tag{A16}$$

The projection of a rotated version of the image, f(x,y), can be Fourier-transformed in one dimension to obtain the 2-D Fourier transform of the image in cylindrical coordinates, evaluated along a constant-θ slice in the frequency domain. This result is known as the projection-slice theorem (Munson et al. 1983). It implies that a sequence of projections of incrementally rotated images can be used to obtain a sequence of constant-θ slices of the 2-D Fourier transform of the image in cylindrical coordinates. The image can be reconstructed from its projections by computing an inverse 2-D Fourier transform in cylindrical coordinates, as in equation (A7). This form of reconstruction is known as back projection.

To obtain a more explicit expression for the reconstructed image in terms of its projections, equation (A16) is solved for $P_\theta(x)$ by taking the inverse 1-D Fourier transform of both sides of the equation,

$$P_\theta(x) = (2\pi)^{-1}\int_{-\infty}^{\infty} F_{cyl}(r,\theta)\exp(jrx)dr. \tag{A17}$$

A gradual high-pass filter (similar to differentiation without the corresponding phase shift) can be applied to the projection, yielding

$$P_{\theta,HP}(x) = (2\pi)^{-1}\int_{-\infty}^{\infty} F_{cyl}(r,\theta)\exp(jrx)|r|dr. \tag{A18}$$

The integral on the right-hand side of equation (A18) is contained in the 2-D inverse Fourier transform expression, equation (A7), in the form

$$(2\pi)^{-1}\int_{-\infty}^{\infty} F_{cyl}(r,\theta)\exp[jr\rho\cos(\theta-\phi)]|r|dr = P_{\theta,HP}[\rho\cos(\theta-\phi)]. \tag{A19}$$

Substituting equaiton (A19) into equation (A7) yields

$$f_{cyl}(\rho,\phi) = (2\pi)^{-1}\int_{-\pi/2}^{\pi/2} P_{\theta,HP}[\rho\cos(\theta-\phi)]d\theta. \tag{A20}$$

The original image, $f_{cyl}(\rho,\phi)$, can be reconstructed by summing high-pass filtered projections. To obtain the image, f(x,y), in Cartesian coordinates, recall from equation (A3) that

$$f_{cyl}(\rho,\phi) \equiv f(\rho\cos\phi, \rho\sin\phi) = f(x,y)$$

and from equation (A6) that

$$\cos(\theta-\phi) = \cos\theta\cos\phi + \sin\theta\sin\phi..$$

It follows that equation (A20) can be written as

$$f(\rho\cos\phi,\rho\sin\phi) = (2\pi)^{-1}\int_{-\pi/2}^{\pi/2} P_{\theta,HP}[(\rho\cos\phi)\cos\theta + (\rho\sin\phi)\sin\theta]d\theta \qquad \text{(A21)}$$

or

$$f(x,y) = (2\pi)^{-1}\int_{-\pi/2}^{\pi/2} P_{\theta,HP}(x\cos\theta + y\sin\theta)d\theta\,. \qquad \text{(A22)}$$

Back projection algorithms typically utilize the projection-slice theorem to obtain the 2-D Fourier transform of the image in cylindrical coordinates. The image is then reconstructed via a 2-D inverse Fourier transform operation. The equivalent expression in equation (A22), however, is useful for illustrating the similarity between back projection and synthetic aperture processing.

For radar/sonar/ultrasound processing, suppose that a transducer is placed on the negative x-axis. A target is rotated about the origin of the coordinate system, and the range is defined to be zero at the center of rotation. Projections of the target are obtained by rotating the target clockwise and recording reflectivity vs. range (A-scan) data at each rotation after filtering to obtain an estimate of the target impulse response (e.g., matched filtering). The integration surfaces for each projection correspond to points with constant delay (e.g., spherical shells). The thickness of the integration surfaces or shells are determined by the range resolution cell of the system (i.e., by the system bandwidth).

To track a point on the target with initial position (x,y), the matched filtered echo (A-scan) from the target is evaluated at range $x\cos\theta+y\sin\theta$ as the target is rotated. Equation (A22) describes a sum of high pass, matched filtered echoes from the point on the target at initial position (x,y) as the target is rotated.

The same A-scan data can be obtained by moving the transducer in a circle around the target, or by using a large array of transducers that are arranged in a circle with the target at the center. The second alternative is an actual array, while the first is a synthetic array. The array is focused on a target point by delay-and-sum beam forming. Consider a transducer that is located on a circle, θ radians counterclockwise relative to the negative x-axis. A signal is transmitted toward the target from this transducer, and the resulting echo is received by the same transducer and matched filtered or otherwise processed to estimate target impulse response. The contribution of this filtered transducer output to the beam former image of the target point at x,y is a sample of the matched filtered echo. This sample is chosen to correspond to the range of the target point (i.e., to a range of $x\cos\theta+y\sin\theta$ when range zero is at the center of the circle). The delay-and-sum beam former for the real or synthetic array approximates the integral in equation (A22) by a finite sum over a sequence of aspect (θ) values. Such a finite sum approximation is also used in back projection. If the matched filtered echoes are high-pass filtered by using a filter with transfer function, $|\omega|$, synthetic aperture imaging and back projection are equivalent processes.

One way to exploit the equivalence of SAS and BP is to form a 3-D image when the transducer is above the plane of rotation. If the transducer is located above the negative x-axis such that the line between the transducer and the origin forms an angle, α, relative to the negative x-axis, and if the target is in the far field of the transducer, then equation (A22) becomes

$$f(x,y,z) = (2\pi)^{-1}\int_{-\pi/2}^{\pi/2} P_{\theta,HP}[(x\cos\theta + y\sin\theta)\cos\alpha - z\sin\alpha]d\theta\,. \qquad \text{(A23)}$$

REPORT DOCUMENTATION PAGE

Form Approved
OMB No. 0704-0188

1. AGENCY USE ONLY *(Leave blank)*	2. REPORT DATE	3. REPORT TYPE AND DATES COVERED
	January 1998	Final

4. TITLE AND SUBTITLE

TOMOGRAPHIC IMAGE RECONSTRUCTION OF MCM TARGETS USING DOLPHIN SYNTHETIC SIGNALS

5. FUNDING NUMBERS

PE: 0602315N
AN: DN303032
CN: N6001–97–M–U033

6. AUTHOR(S)

R. A. Altes, Chirp Corporation
P. W. Moore, D. Helweg, SSC San Diego

7. PERFORMING ORGANIZATION NAME(S) AND ADDRESS(ES)

Chirp Corporation
8248 Sugarman Drive
La Jolla, CA 92037

8. PERFORMING ORGANIZATION REPORT NUMBER

TD 2993

9. SPONSORING/MONITORING AGENCY NAME(S) AND ADDRESS(ES)

Office of Naval Research
800 North Quincy Street
Arlington, VA 22219–5660

Space and Naval Warfare Systems Center
San Diego, CA 92152–5001

10. SPONSORING/MONITORING AGENCY REPORT NUMBER

11. SUPPLEMENTARY NOTES

12a. DISTRIBUTION/AVAILABILITY STATEMENT

Approved for public release; distribution is unlimited.

12b. DISTRIBUTION CODE

13. ABSTRACT *(Maximum 200 words)*

Synthetic aperture sonar/radar (SAS/SAR) imaging and back projection (BP) acoustic tomography are identical processes if echoes are appropriately filtered. This equivalence has several important implications. First, the point spread function of a BP image is equivalent to the range, cross-range ambiguity function (RCAF) of the SA system. Any process that makes the RCAF more like a two-dimensional impulse will improve image quality. The rotated wavelet transform, for example, yields an impulse-like RCAF even for sparse angular sampling. The waveforms and beam patterns for rotated wavelet imaging resemble those used by an echolocating dolphin. Tradeoffs between system bandwidth and angular observation interval can be predicted from the RCAF. The SAS/BP equivalence also implies that part of a BP image can be constructed without having to construct the whole image.

Another implication is that a high-resolution BP "feature image" can be constructed. A feature image is a generalization of conventional reflectivity vs. position. Reflectivity is replaced by a feature that represents surface roughness, for example. Synthetic aperture processing can also be used to construct a three-dimensional (3-D) BP image when the sonar is above the plane of target rotation. Applications include clutter/speckle suppression via feature images, better focusing via a composite 2-D image that combines a set of range-azimuth images from different evaluations, and a 3-D representation of an object's surface (as opposed to its reflectivity), thus permitting a sonar system to synthesize a 3-D vision-like target image. These applications are illustrated with examples derived using sonar backscatter from a very shallow water (VSW) mine simulator ensonified with synthetic broadband bottlenose dolphin echolocation clicks.

14. SUBJECT TERMS

Mission Area: Marine Mammals
mine detection sonar
imaging

15. NUMBER OF PAGES

26

16. PRICE CODE

17. SECURITY CLASSIFICATION OF REPORT	18. SECURITY CLASSIFICATION OF THIS PAGE	19. SECURITY CLASSIFICATION OF ABSTRACT	20. LIMITATION OF ABSTRACT
UNCLASSIFIED	UNCLASSIFIED	UNCLASSIFIED	SAME AS REPORT

21a. NAME OF RESPONSIBLE INDIVIDUAL	21b. TELEPHONE *(include Area Code)*	21c. OFFICE SYMBOL
P. W. Moore	(619) 553-0888 email: pmoore@spawar.navy.mil	Code D351

INITIAL DISTRIBUTION

Code D0012	Patent Counsel	(1)
Code D0271	Archive/Stock	(6)
Code D0274	Library	(2)
Code D027	M. E. Cathcart	(1)
Code D0271	D. Richter	(1)
Code D35	J. Haun	(1)
Code D351	D. Helweg	(100)
Code D352	R. Kataoka	(1)
Code D3501	M. Rothe	(1)
Code D3503	S. Ridgway	(1)

Defense Technical Information Center
Fort Belvoir, VA 22060–6218 (4)

SPAWARSYSCEN Liaison Office
Arlington, VA 22202–4804

Center for Naval Analyses
Alexandria, VA 22302–0268

Navy Acquisition, Research and Development
Information Center (NARDIC)
Arlington, VA 22244–5114

GIDEP Operations Center
Corona, CA 91718–8000